Supporting Information

Electron-mediator-free efficient photocatalytic regeneration of coenzyme NAD(P)H via direct electron transfer using ultrathin Bi_2MoO_6 nanosheets

Yao Chai,[a] Zirui Pang,[a] Heng Jiang,[a] Chi Chung Tsoi,[a] Liang Wan,[a] Yu Du,[a] Huaping Jia,[a] Yujiao Zhu,[a] Detao Liu,[d] Fengjia Xie,[*,a] Guangya Zhou[*,c] and Xuming Zhang[*,a,b]

E-mail: xuming.zhang@polyu.edu.hk, mpezgy@nus.edu.sg, fengjia.xie@connect.polyu.hk.

CONTENTS

EXPERIMENTAL

Materials: Hexadecyltrimethylammonium bromide [$CH_3(CH_2)_{15}N(Br)(CH_3)_3$, ≥98%], Bismuth(III) nitrate pentahydrate [$Bi(NO_3)_3{\cdot}5H_2O$, ACS reagent, ≥98.0%], Sodium molybdate dihydrate [$Na_2MoO_4{\cdot}2H_2O$, ACS reagent, ≥99%], β-Nicotinamide adenine dinucleotide hydrate (NAD^+, ≥99%), β-Nicotinamide adenine dinucleotide, reduced disodium salt hydrate (β-NADH, ≥97%), β-Nicotinamide adenine dinucleotide phosphate hydrate (β-$NADP^+$, ≥95%), Pentamethylcyclopentadienylrhodium(III) chloride dimer [$(Cp^*RhCl_2)_2$, ≥97%], and 2, 2'-Bipyridyl ($C_{10}H_8N_2$, ≥99%) were purchased from Sigma-Aldrich Chemical Reagent Co.,Ltd.

Characterization: The crystal structure of each photocatalyst was analyzed using X-ray powder diffractometer (XRD, Rigaku SmartLab). Transmission electron microscopy (TEM, FEI TS12) was utilized to examine the microscopic morphology of the photocatalysts. X-ray photoelectron spectroscopy (XPS) and ultraviolet photoelectron spectroscopy (UPS) were conducted with a Thermo ESCALAB 250XI instrument and a Thermo ESCALAB Xi+ instrument equipped with an ultraviolet photoelectron spectroscope (He I, 21.22 eV), respectively. Furthermore, the ultraviolet-visible diffuse reflectance spectra (UV-vis DRS) of the catalysts were acquired on a PerkinElmer UV-vis-NIR spectrometer equipped with an integrating sphere. The scanning range was set at 250-800 nm, with a measurement rate of 2 nm/s. Atomic force microscopy (AFM) data were collected using a Bruker Dimension edge. Additionally, photoluminescence (PL) spectra and time-resolved photoluminescence (TRPL) spectra were obtained on an Edinburgh fluorescence spectrometer (PLS1000). N_2 adsorption–desorption isotherms at 77 K were conducted on a Micrometrics ASAP2460 analyzer.

Photoelectrochemical Measurements: The CHI660 electrochemical workstation was used to evaluate the photoelectric properties of the catalyst, providing insights into the separation and migration of photo-generated carriers. A dispersion containing 10 mg of photocatalyst and 20 μL of 5% Nafion solution in 1 mL ethanol underwent 3 hours of sonication. Subsequently, 20 μL of the resulting solution was applied to the conductive surface of a glass electrode with a diameter of approximately 0.25 cm and allowed to air dry. The remaining conductive glass was uniformly coated with nail polish to prevent unintended photoelectric signals. For photocurrent measurements, Pt plates served as the counter electrode, Ag/AgCl as the reference electrode, and Na_2SO_4 (0.2 M) as

the electrolyte solution. For electrochemical impedance measurements, a 0.5 M KCl solution with 5.0 mM $K_3[Fe(CN)_6]/K_4[Fe(CN)_6]$ was used as the electrolyte solution.

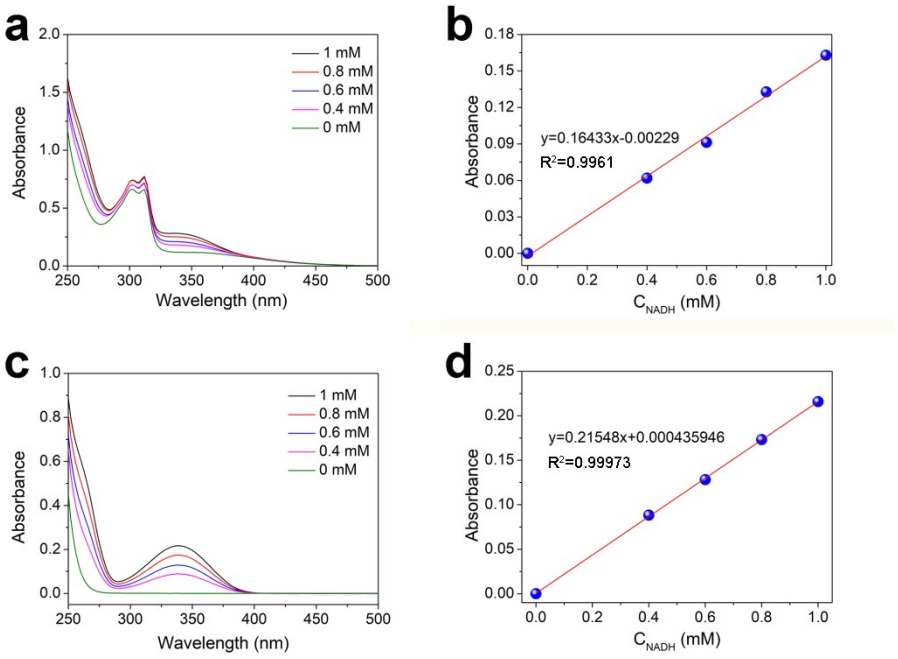

Fig. S1. (a) UV-visible absorption spectra of of NADH at different concentrations in an environment containing an electron mediator and (b) the corresponding standard curve. (c) UV-visible light absorption spectra of NADH at different concentrations in an environment without electron mediator and (d) the corresponding standard curve.

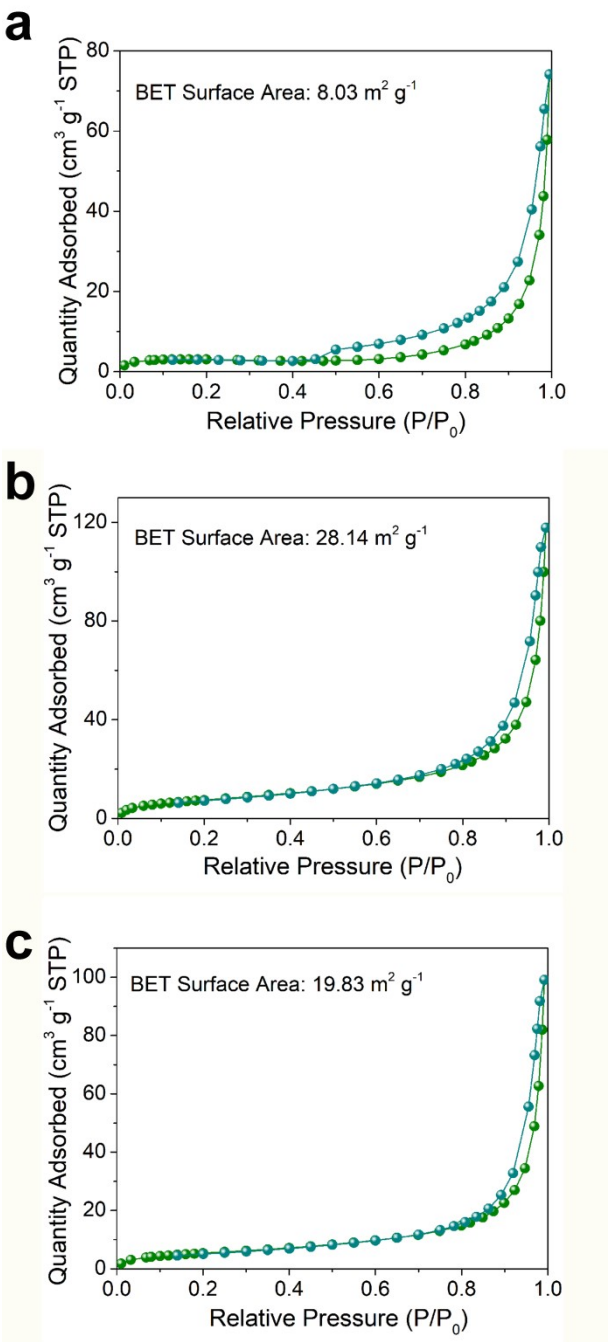

Fig. S2. Nitrogen adsorption-desorption curves of a series of catalysts at different preparation temperatures: (a) BMO-80, (b) BMO-100, and (c) BMO-120.

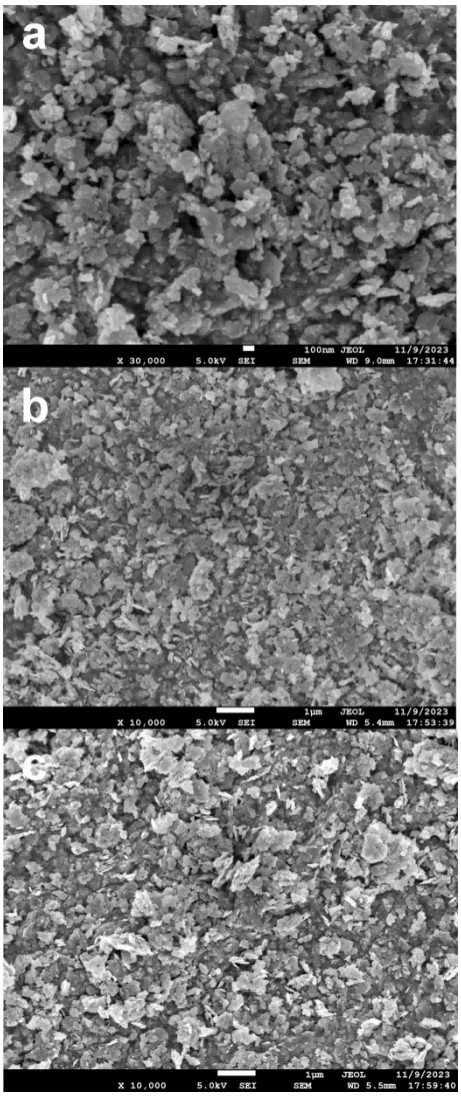

Fig. S3. SEM of Bi_2MoO_6 nanosheets under various hydrothermal preparation temperatures. (a) BMO-80, (b) BMO-100, (c) BMO-120.

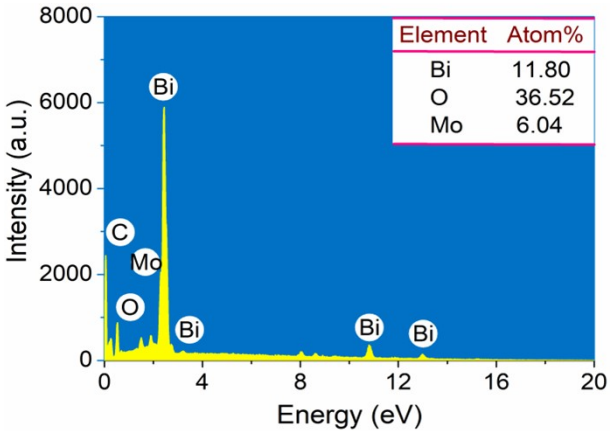

Fig. S4. Typical EDS spectrum of the BMO-100 sample.

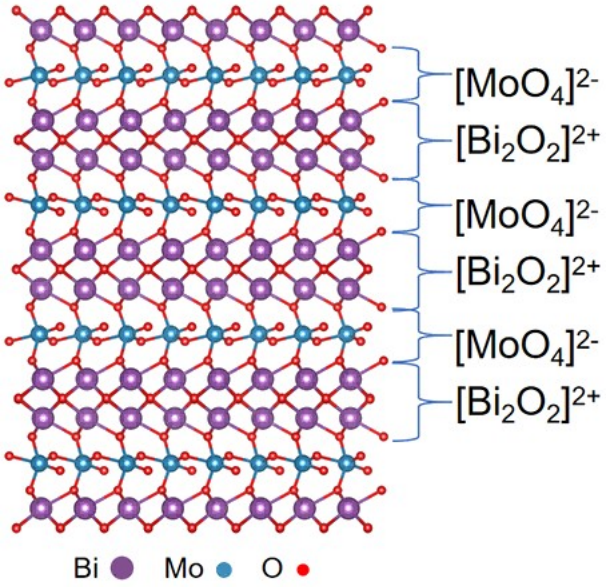

Fig. S5. Schematic diagram of Bi_2MoO_6 crystal structure.

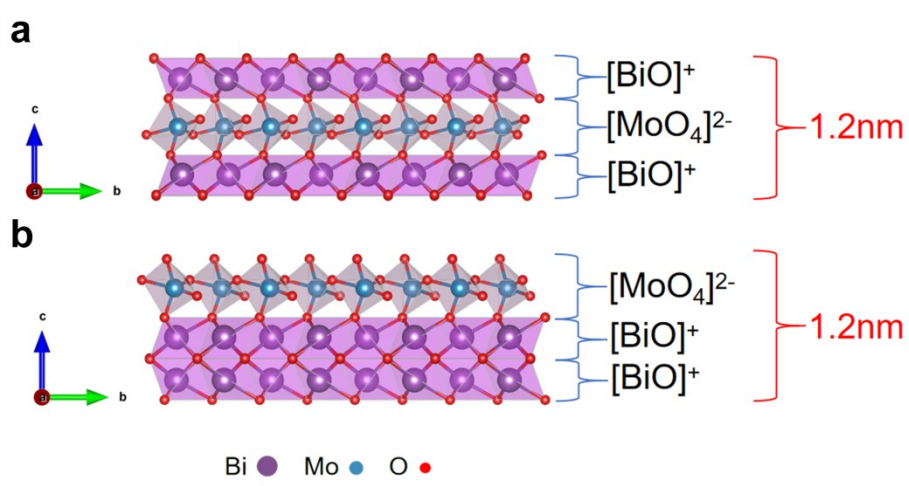

Fig. S6. Schematic representation of two possible structures possible for a single layer of Bi_2MoO_6. (a) $[BiO]^+$–$[MoO_4]^{2-}$–$[BiO]^+$ sandwich structure and (b) $[MoO_4]^{2-}$–$[BiO]^+$–$[BiO]^+$ non-sandwich structure.

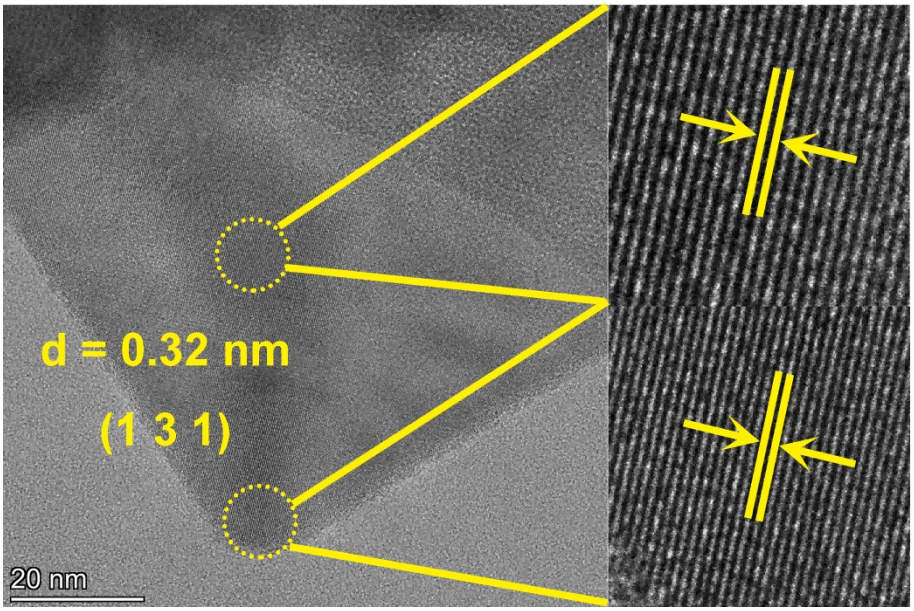

Fig. S7. HRTEM image of BMO-100.

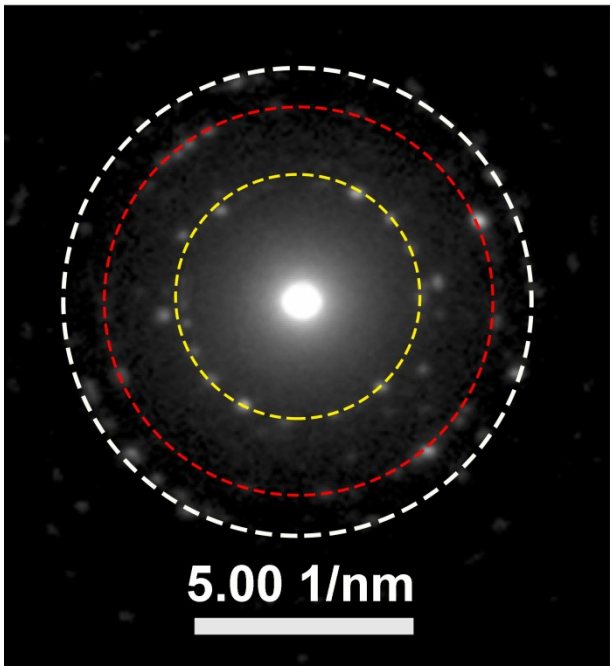

Fig. S8. SAED image of BMO-100.

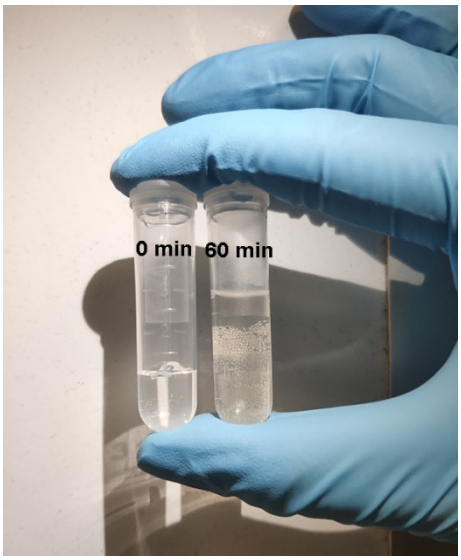

Fig. S9. The color of the reaction solution changed gradually over time.

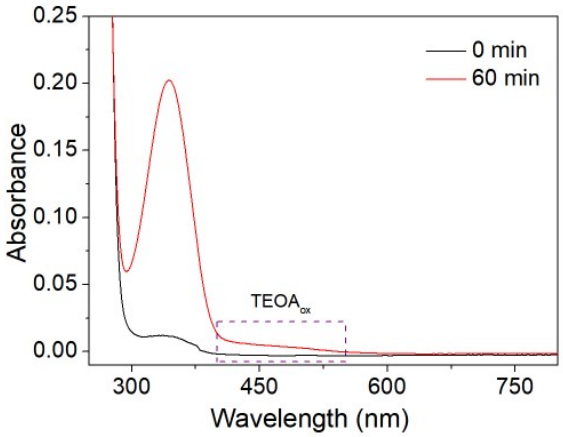

Fig. S10. UV-visible absorption spectrum of photocatalytic NADH regeneration by BMO-100.

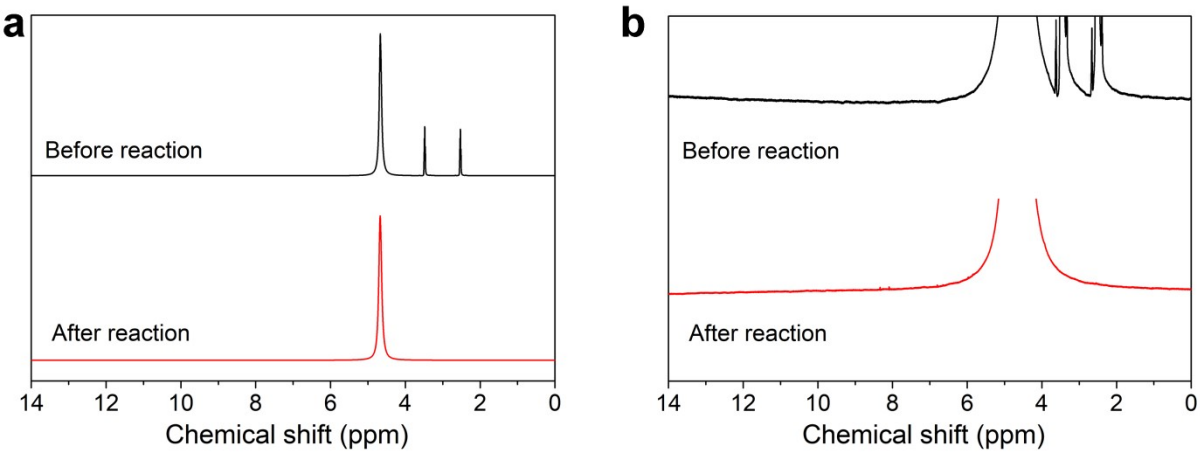

Fig. S11. Photocatalytic TEOA oxidation. NMR spectra before and after the reaction and the enlarged image.

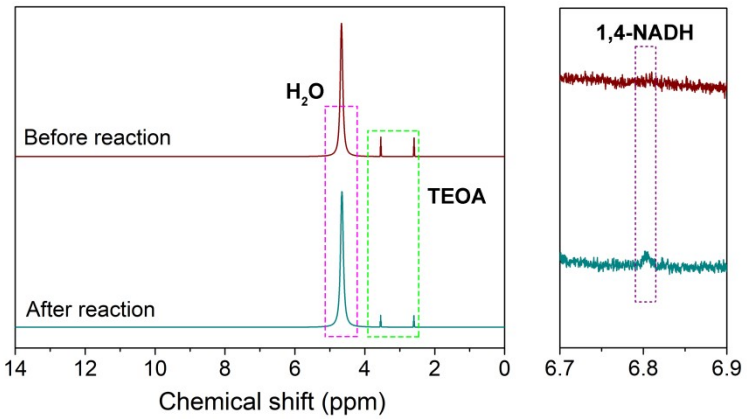

Fig. S12. ^{1}H NMR spectra of the solution before and after 1 hour of illumination, along with the enlarged spectrum.

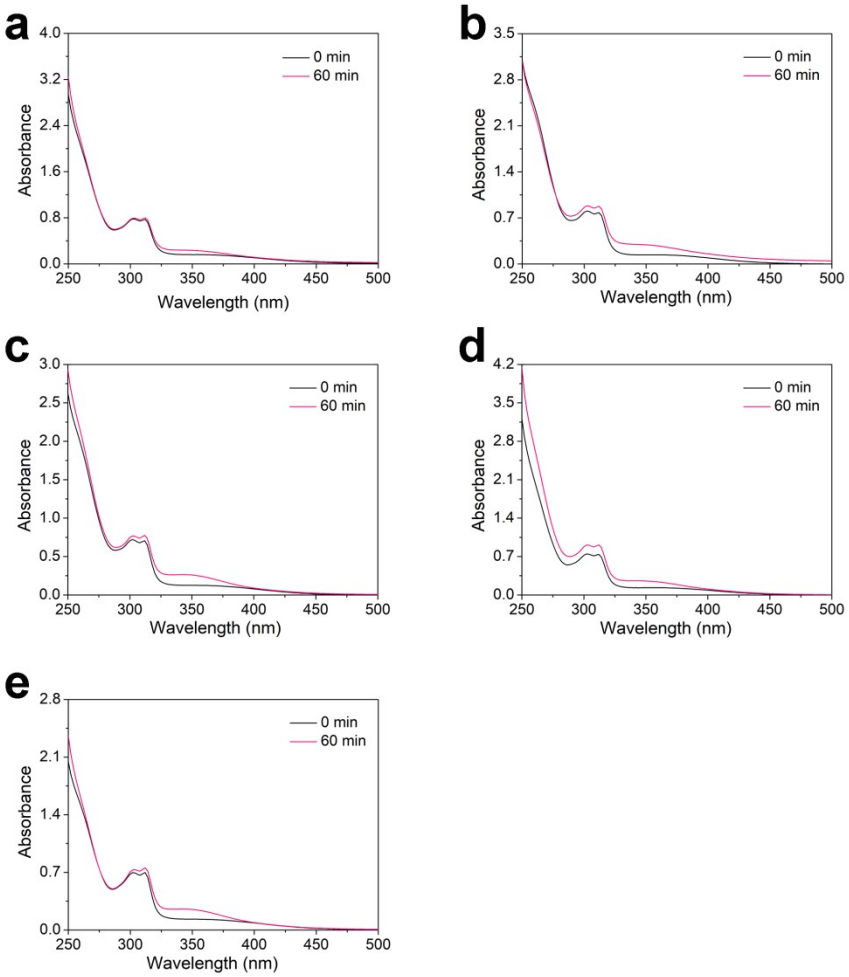

Fig. S13. UV-Vis absorption spectra of photocatalytic NADH regeneration over a series of photocatalysts in the presence of electron mediators. (a) BMO-80, (b) BMO-100, (c) BMO-120, (d) BMO-140, and (e) BMO-160.

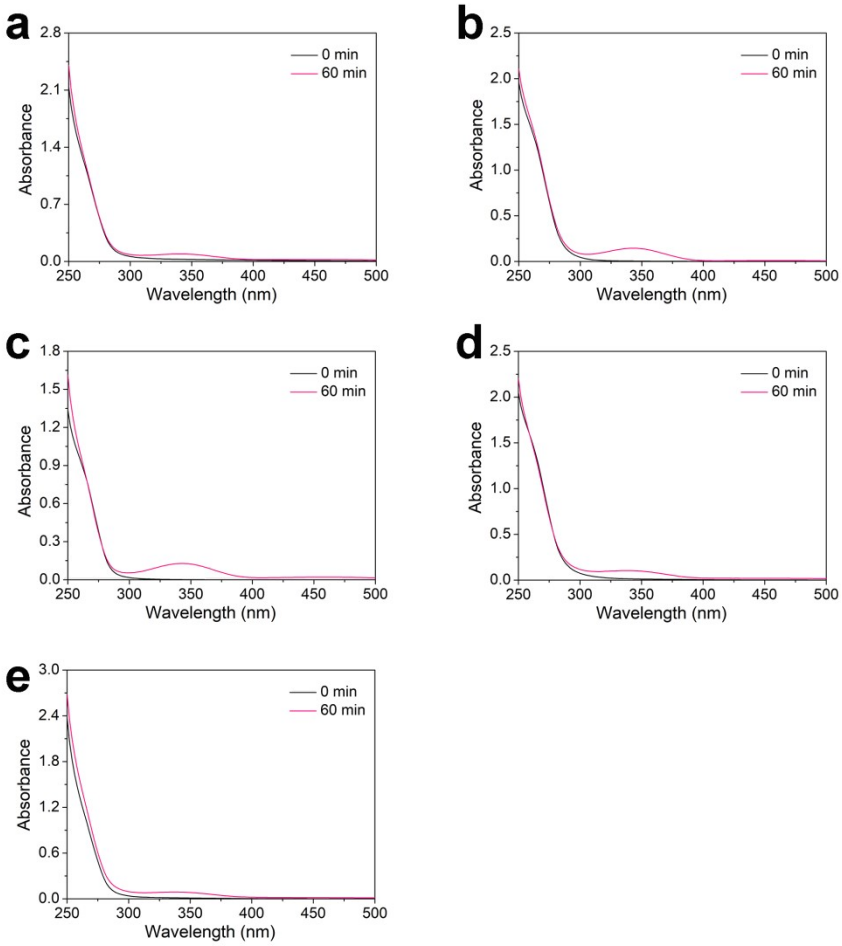

Fig. S14. UV-Vis absorption spectra of photocatalytic NADH regeneration over a series of photocatalysts in the absence of electron mediators. (a) BMO-80, (b) BMO-100, (c) BMO-120, (d) BMO-140, and (e) BMO-160.

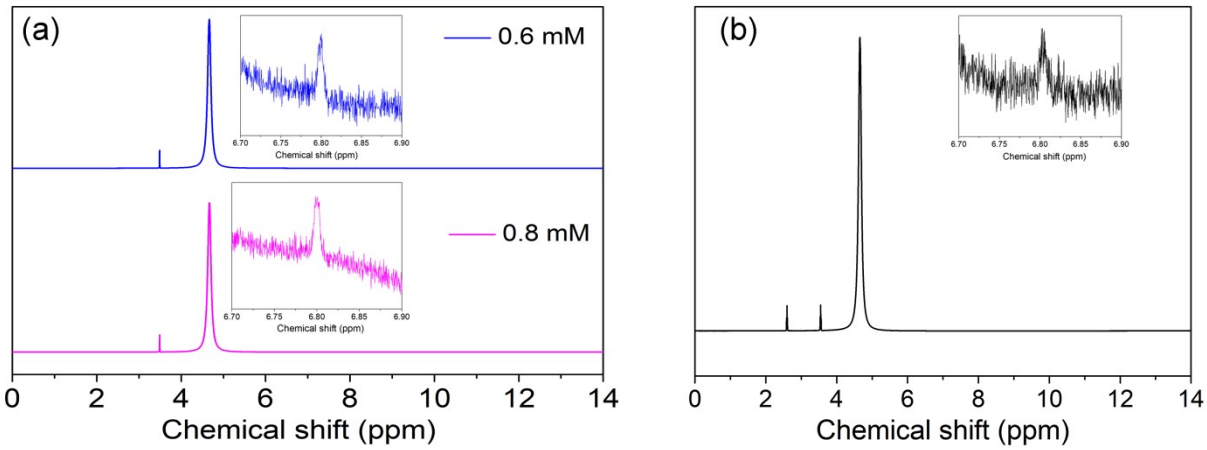

Fig. S15. (a) ^{1}H NMR spectra of NADH standard solutions with different concentrations and the enlarged image. (b) ^{1}H NMR spectra of the solution after 1 hour of illumination, along with the enlarged spectrum.

To ensure accuracy in the NMR analysis, we utilized the distinct ^{1}H NMR signal of 1,4-NADH, observed at 6.8 ppm, as a marker for NADH concentration. We established a direct relationship between 1,4-NADH concentration and its peak area at 6.8 ppm. Specifically, at a concentration of 0.6 mM, the peak area measured was 2.2212×10^{-4}, and at 0.8 mM, it was 2.6268×10^{-4}. Using this calibration, we determined the NADH concentration post-regeneration with the BMO-100 photocatalyst. The peak area at 6.8 ppm was approximately 2.1620×10^{-4}, corresponding to a concentration of 0.62 mM.

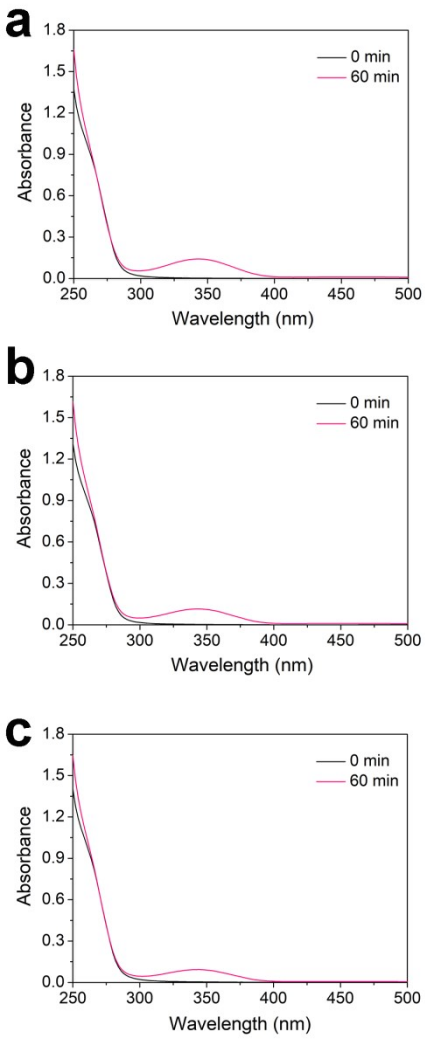

Fig. S16. UV-visible absorption spectra of photocatalytic NADH regeneration by BMO-100 under different monochromatic light irradiations: (a) 380 nm, (b) 400 nm, (c) 420 nm.

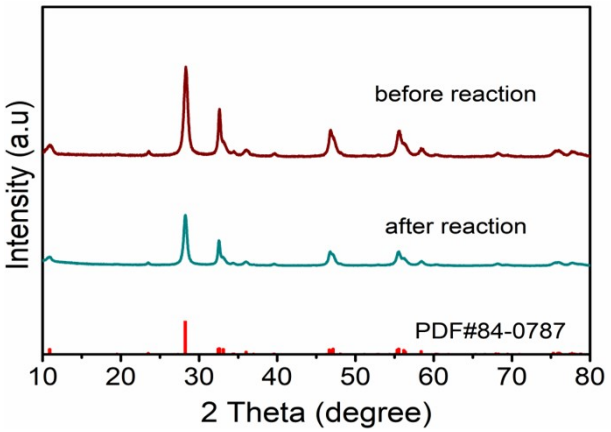

Fig. S17. XRD patterns of catalyst before and after cycle.

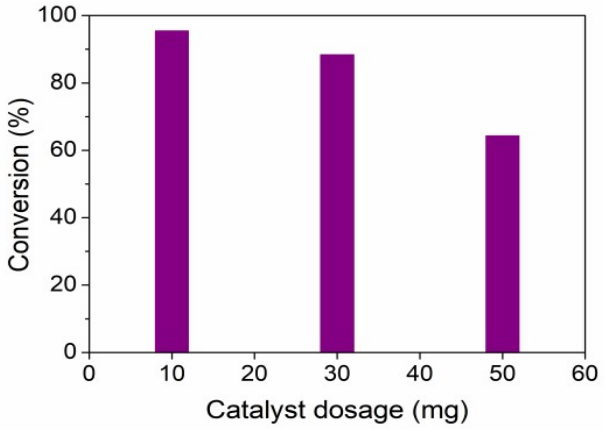

Fig. S18. Effect of catalyst dosage on photocatalytic NADH regeneration activity.

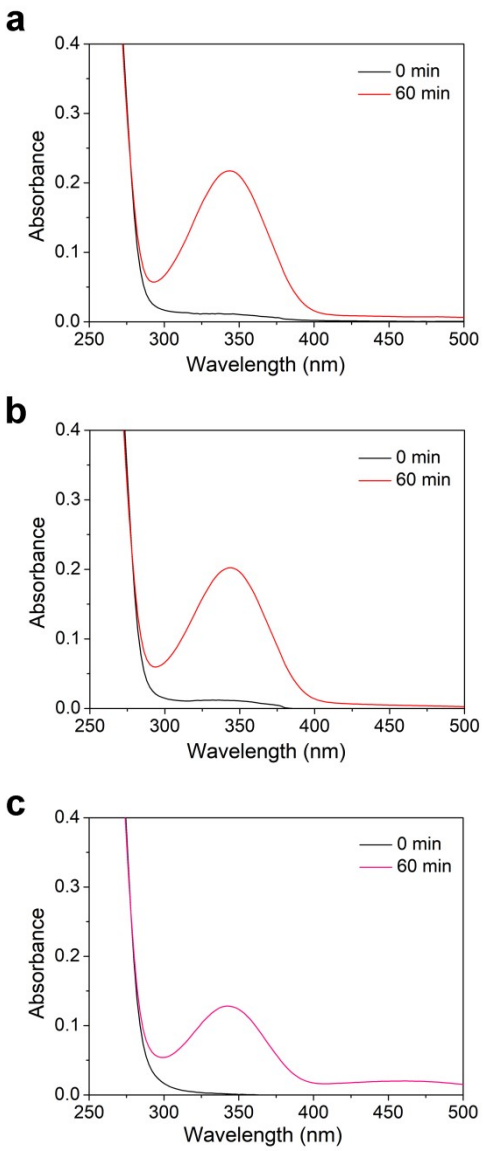

Fig. S19. UV-Vis absorption spectra of photocatalytic NADH regeneration with different amounts of catalyst.

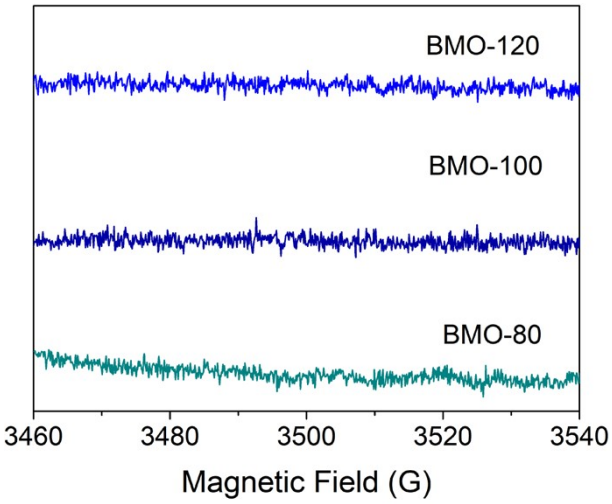

Fig. S20. EPR signal of defective structures.

Table S1. Calculation of PMI during catalyst preparation.

Type	Reactants	Reagents	Solvent	Product
Name	$Na_2MoO_4 \cdot 2H_2O$, $Bi(NO_3)_3 \cdot 5H_2O$	CTAB	H_2O	Bi_2MoO_6
Mass/g	0.24195 + 2×0.485.07	0.05	330	0.6
PMI	(0.24195 + 2×0.485.07 + 0.05 + 330)/0.6 = 552.10			

Table S2. Comparison of PMI of different catalytic systems.

Reactants	Reagents	Solvents	Catalyst	Product	PMI	Ref.
NAD^+	TEOA	PBS	Bi_2MoO_6	NADH	**9211.98**	This work
6.6343×10^{-4}	0.15	4	0.05	4.56×10^{-4}		
NAD^+	TEOA, HCl or NaOH	PBS	PDA/g-C_3N_4	NADH	**＞6191**	40
6.6343×10^{-4}	＞0.15	＞4	0.01	6.72×10^{-4}		
NAD^+	TEOA	PBS	Lawn-like TP-COFs/$Ti_3C_2T_x$	NADH	**34112**	44
6.6343×10^{-4}	0.15	10	0.015	2.98×10^{-4}		
NAD^+	EDTA-2Na, EDTA-4Na, TEOA, lactic acid or pure H_2O		ARTM36	NADH	**32583**	45
6.6343×10^{-4}	15		0.020	4.61×10^{-4}		